THE JOURNAL OF PHYSICAL CHEMISTRY Letters

Letter

pubs.acs.org/JPCL

How Cubic Can Ice Be?

Andrew J. Amaya,[†] Harshad Pathak,[†] Viraj P. Modak,[†] Hartawan Laksmono,[‡] N. Duane Loh,[‡,∥] Jonas A. Sellberg,[‡,#,●,⊥] Raymond G. Sierra,[‡] Trevor A. McQueen,[⊥,+] Matt J. Hayes,[◆] Garth J. Williams,[◆,▽] Marc Messerschmidt,[◆,¶] Sébastien Boutet,[◆] Michael J. Bogan,[‡] Anders Nilsson,[‡,#,§] Claudiu A. Stan,[*,‡] and Barbara E. Wyslouzil[*,†,○]

[†]William G. Lowrie Department of Chemical and Biomolecular Engineering, Ohio State University, Columbus, Ohio 43210, United States

[‡]Stanford PULSE Institute, SLAC National Accelerator Laboratory, Menlo Park, California 94025, United States

[∥]Department of Physics, National University of Singapore, Singapore 117557

[#]Department of Physics, AlbaNova University Center, Stockholm University, S-106 91 Stockholm, Sweden

[●]Biomedical and X-ray Physics, Department of Applied Physics, AlbaNova University Center, KTH Royal Institute of Technology, S-106 91 Stockholm, Sweden

[⊥]SUNCAT Center for Interface Science & Catalysis, SLAC National Accelerator Laboratory, Menlo Park, California 94025, United States

[+]Department of Chemistry, Stanford University, Stanford, California 94305, United States

[◆]Linac Coherent Light Source, SLAC National Accelerator Laboratory, Menlo Park, California 94025, United States

[▽]Brookhaven National Laboratory, Upton, New York 11973, United States

[¶]National Science Foundation BioXFEL Science and Technology Center, Buffalo, New York 14203, United States

[§]Stanford Synchrotron Radiation Lightsource, SLAC National Accelerator Laboratory, Menlo Park, California 94025, United States

[○]Department of Chemistry and Biochemistry, Ohio State University, Columbus, Ohio 43210, United States

Supporting Information

ABSTRACT: Using an X-ray laser, we investigated the crystal structure of ice formed by homogeneous ice nucleation in deeply supercooled water nanodrops ($r \approx 10$ nm) at ~225 K. The nanodrops were formed by condensation of vapor in a supersonic nozzle, and the ice was probed within 100 μs of freezing using femtosecond wide-angle X-ray scattering at the Linac Coherent Light Source free-electron X-ray laser. The X-ray diffraction spectra indicate that this ice has a metastable, predominantly cubic structure; the shape of the first ice diffraction peak suggests stacking-disordered ice with a cubicity value, χ, in the range of 0.78 ± 0.05. The cubicity value determined here is higher than those determined in experiments with micron-sized drops but comparable to those found in molecular dynamics simulations. The high cubicity is most likely caused by the extremely low freezing temperatures and by the rapid freezing, which occurs on a ~1 μs time scale in single nanodroplets.

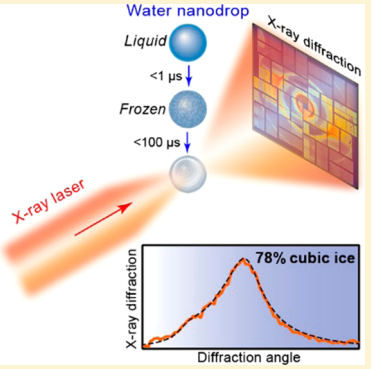

Freezing in a supercooled liquid is a nonequilibrium process and may proceed through metastable solid phases in accordance with Ostwald's rule of stages.[1,2] These metastable solid states can become kinetically trapped, forming glasses as well as materials with metastable crystalline structures or metastable microstructures, such as an ultrafine grain size.[3]

The formation of atmospheric precipitation can include the freezing of supercooled water droplets in clouds,[4] but the crystal structure of the ice that forms in the atmosphere is still debated.[5−8] Although hexagonal ice is the stable polymorph,[9] observations of haloes around the sun and the presence of ice crystals with 3-fold rotational symmetry points suggest that cubic or stacking-disordered ice may also exist in the atmosphere.[10,11] The possible presence of this metastable form of ice is important because it can affect both the water vapor content and the optical properties of ice clouds.[12−14]

Given the importance that the phase of ice has on atmospheric processes, experiments have studied the structure of ice formed when supercooled water freezes.[15,16] The current consensus is that the first phase that forms is stacking-disordered ice, that is, ice that is comprised of interlaced cubic and hexagonal sequences of two-dimensional ice layers; this phase anneals to stable hexagonal ice, and in micron-sized samples, the annealing time ranges from minutes near melting temperatures to hours at homogeneous nucleation temper-

Received: May 9, 2017
Accepted: June 28, 2017
Published: June 28, 2017

DOI: 10.1021/acs.jpclett.7b01142
J. Phys. Chem. Lett. 2017, 8, 3216−3222

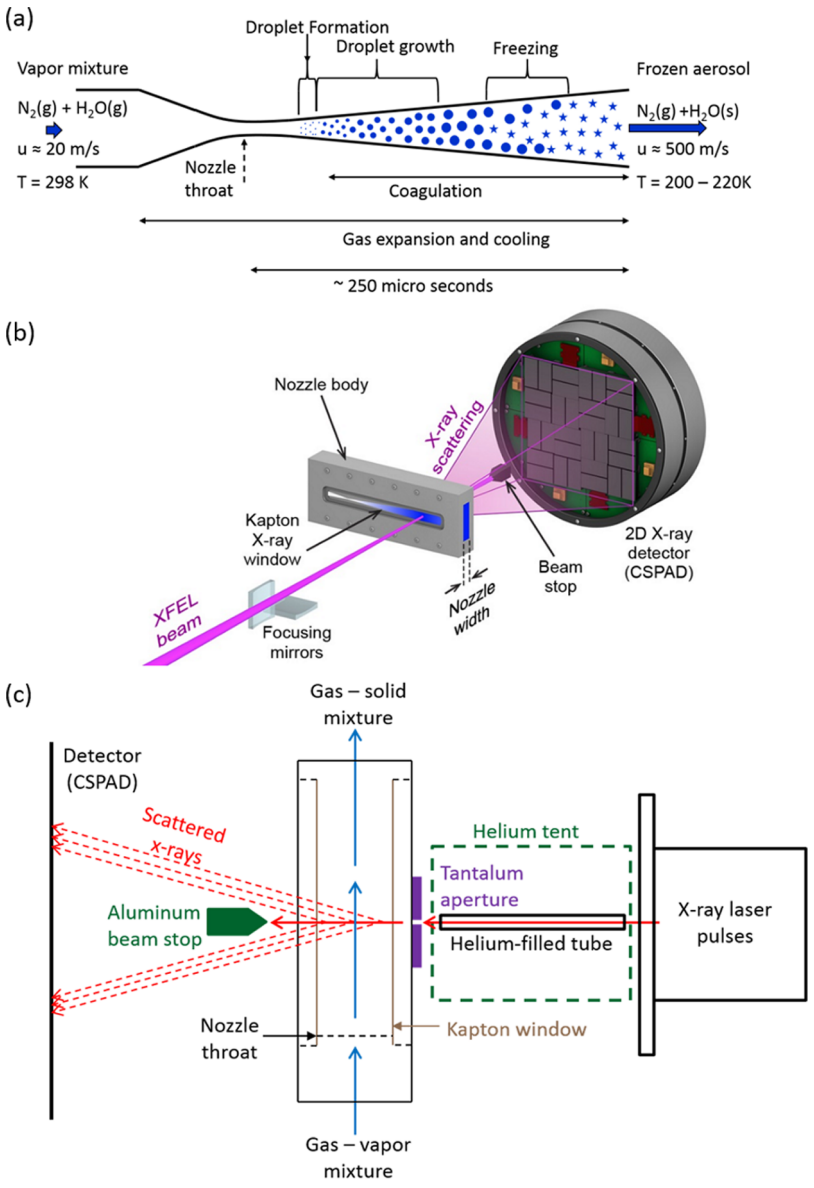

Figure 1. (a) As a condensable vapor flows through a converging–diverging nozzle, it cools rapidly and the vapor condenses, forming nanodroplets. Upon further cooling, these droplets can freeze. (b,c) Simplified drawings of the experimental setup for recording X-ray diffraction data at the CXI instrument, SLAC National Laboratory. These schematics are not to scale.

atures.[16−20] Furthermore, the initial stacking-disordered ice contains a larger fraction of cubic sequences, or is more "cubic", when freezing occurs at lower temperatures.[5,18] The degree of ice cubicity χ is equal to the fraction of cubic layers if the stacking is random. A more exact definition[7,15,18,19] of χ that includes stacking memory effects is available in the Supporting Information (SI). Experiments with frozen emulsions[15] and vapor-deposited ice[7] observed a maximum $\chi \approx 0.5$. To date, the ice with the highest reported cubicity, $\chi = 0.733$, was made by the transformation of ice II to ice I.[18]

Numerical simulations of freezing in supercooled water also observed the formation of stacking-disordered ice and its increase in cubicity at lower freezing temperatures,[5,21−24] but they predict a cubicity χ between 0.6 and 0.7, higher than that observed experimentally by freezing micron-sized supercooled drops. This difference in χ might be due to the vastly different conditions probed in experiments versus simulations. In particular, simulations investigate nanosized samples up to microsecond time scales, much shorter than the characteristic time of other experiments.[15] Furthermore, they often probe temperatures below the "homogeneous nucleation limit" of ~235 K, which cannot be reached by most experimental methods.

Here, we report the results of an experiment in which we investigated the freezing of supercooled water under conditions that approach those in simulations: nanosized aerosol droplets that are deeply supercooled and whose structure is determined within microseconds of freezing using in situ diffraction from a high-intensity X-ray laser source.

We produced and then froze nanodroplets of pure water by flowing a mixture of nitrogen carrier gas and water vapor through a converging–diverging supersonic nozzle, illustrated in Figure 1. As the vapor-carrier gas mixture expanded across the nozzle, its temperature decreased at a rate of ~0.5 K/μs, increasing the supersaturation of the vapor until a ~10 μs burst of homogeneous vapor–liquid nucleation produced an aerosol

DOI: 10.1021/acs.jpclett.7b01142
J. Phys. Chem. Lett. 2017, 8, 3216−3222

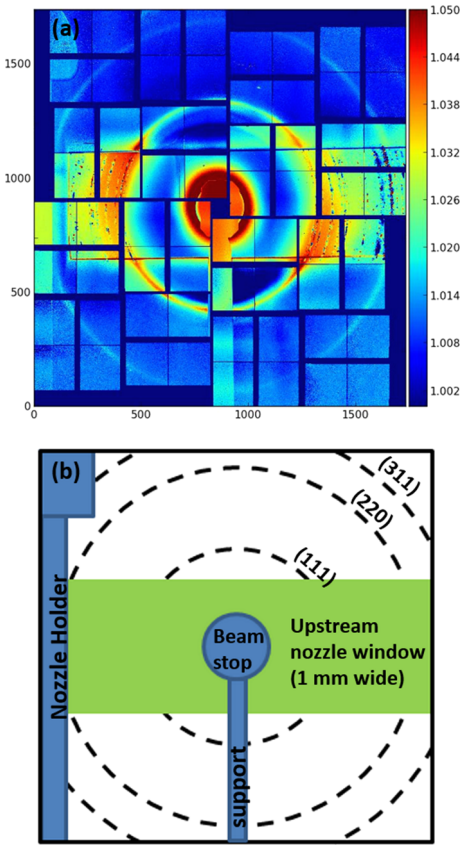

Figure 2. (a) After averaging and background normalization, an image of the processed X-ray scattering pattern exhibits 2−3 concentric rings corresponding to the powder diffraction pattern of ice nanoparticles, as well as spurious features characteristic of the setup. (b) The main spurious features on the detector image include shadows from the beam stop and the nozzle holder. The intense parasitic scattering in the central region is due to scattering that was generated by elements outside of the nozzle and passed through the 1 mm wide upstream window of the nozzle. The downstream window is 3 mm wide, and hence, the shadow on the detector is from the upstream window only.

of liquid nanodroplets with a number density around $\sim 10^{12}$ cm^{-3}. Rapid droplet growth released heat to the flow, quenching nucleation and ensuring a nearly monodisperse droplet size distribution with a radius of $r \approx 10$ nm. Once droplet growth was complete, ~60 μs after peak particle production, the aerosol started to expand and cool again until the temperature of the gas mixture reached ~225 K, when liquid−solid homogeneous nucleation initiated freezing within the droplets. The entire aerosol froze within ~45 μs, and modeling (see the SI for details) suggests that individual droplets froze on a time scale on the order of 1 μs.

We characterized the phase transitions and followed the aerosol's evolution using position-resolved pressure trace measurements (PTMs), Fourier transform infrared spectroscopy (FTIR), and in situ small-angle X-ray scattering (SAXS). The position-resolved SAXS experiments, performed at the 12-ID C beamline at the Advanced Photon Source user facility, characterized the aerosol's average radius, r = 9.9 nm, its distribution width, δr = 2.4 nm, and the mass fraction of condensate, g = 0.01. From the measurements of pressure and condensate fraction, an integrated data analysis approach[25−27] yielded the distribution along the nozzle of the temperature T, density ρ, gas velocity u, and area ratio A/A^*. Position-resolved FTIR measurements provided the fractions of liquid and frozen aerosol and yielded the onset freezing temperature as well as the time required for all of the droplets in the nozzle to freeze.

The supersonic nozzle and associated characterization techniques provide a robust experimental system with which to reproducibly investigate the liquid-to-solid phase transition of water in very small samples ($\sim 3 < r/\text{nm} < \sim 10$) and at temperatures (202−225 K) that are usually considered to be in the experimental "no man's land" of water.[25,28]

To determine the crystalline structure of the solid particles, we used wide-angle X-ray scattering (WAXS) because X-rays can penetrate through the carrier−aerosol mixture in the nozzle. Given the low volume fraction ($\sim 10^{-6}$) of condensed water in the nozzle and the small scattering probability of X-rays by water, a high-intensity X-ray source, that is, a synchrotron or an X-ray free-electron laser (XFEL), is needed to collect diffraction data in a practical amount of time. XFELs may be a better choice because, although their average photon flux is comparable to the one achievable at high-flux synchrotron setups, XFEL beams can be focused tightly while preserving the photon flux, leading to higher intensities, which we found to improve the signal-to-background ratio (see the SI for a comparison of XFEL and synchrotron measurements). Also, XFEL capabilities are advancing rapidly; for example, average fluxes ~100 times larger than the current best will become available soon at the European XFEL,[29] and a similar increase in flux is planned for the LCLS-II X-ray laser.[30]

We conducted XFEL WAXS experiments at the Linac Coherent Light Source[31] (LCLS) user facility at the SLAC National Accelerator Laboratory. The experimental setup, shown in Figure 1b,c, was installed at the Coherent X-ray

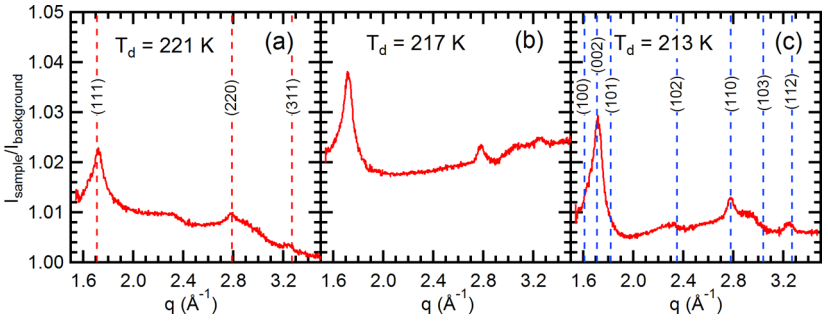

Figure 3. Three X-ray diffraction spectra for ice nanoparticles, taken at positions along the nozzle that correspond to three distinct temperatures. The scattering vector q is related to the scattering angle θ and the X-ray wavelength λ by $q = (4\pi/\lambda)\sin(\theta/2)$. In (a), the red dashed lines correspond to the indicated diffraction peaks of cubic ice. In (c), the blue dotted lines correspond to the diffraction peaks of hexagonal ice.

DOI: 10.1021/acs.jpclett.7b01142
J. Phys. Chem. Lett. 2017, 8, 3216−3222

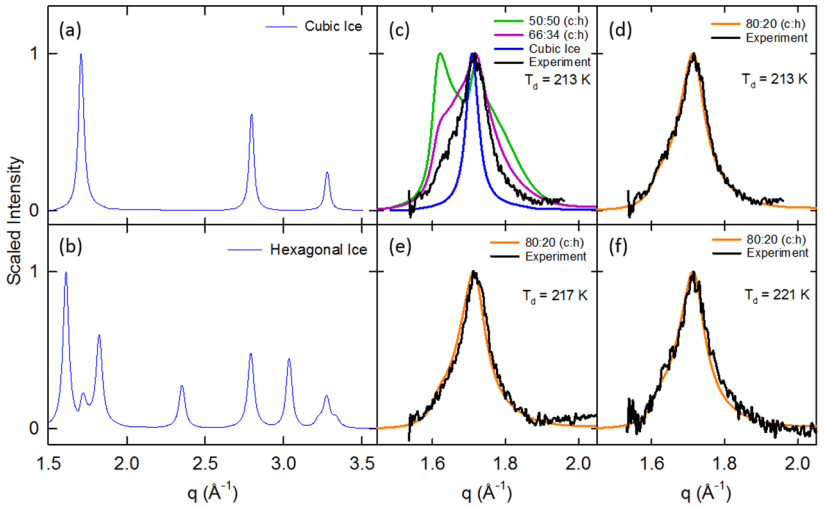

Figure 4. Diffraction spectra calculated using DIFFaX[33] with peak broadening for a particle radius r = 9.9 nm illustrate the difference between (a) cubic and (b) hexagonal ice. The spectrum measured at 213 K is inconsistent with (c) χ = 0.5, 0.66, and 1 but is well fit by (d) χ = 0.8. Panels (e) and (f) illustrate the fits to the data at 217 and 221 K, respectively. All spectra in this figure have been rescaled so that the maximum peak intensity is equal to 1.

Imaging (CXI) end station.[32] The nozzle was mounted in air such that it was directly in the path of X-rays after they were focused by the X-ray focusing mirror, and the diffraction data was collected by a Cornell–SLAC pixel array detector (CSPAD) located approximately 137 mm from the centerline of the nozzle. The X-ray beam with an average photon flux of ~10^{14} photons/s had a wavelength of 1.3 Å, was focused to ~0.1 μm diameter, and was delivered as ~50 fs long pulses of ~10^{12} photons at a pulse rate of 120 Hz.

A significant challenge to our in situ crystal structure determinations was parasitic scattering, which dominated the elastic X-ray scattering from the frozen drops. Parasitic scattering was generated by the air surrounding the nozzle, the N_2 and residual vapor in the nozzle, and the nozzle windows. To minimize air scattering between the beamline's X-ray output window and the nozzle, the beam passed through a helium-filled tube and then through a small aperture in a tantalum plate; we also installed a plastic tent to increase the helium concentration in regions not enclosed by the tube. We used a small nozzle width (0.64 cm) to minimize scattering from the carrier–vapor mixture inside of the nozzle and to avoid excessive geometrical smearing of the diffraction peaks. We note that using helium as a carrier gas would reduce the parasitic scattering but is impractically expensive and that removing the carrier gas would make it difficult to control particle formation and accurately characterize the droplet temperature. Scattering from the nozzle windows, as well as damage to them by the high-intensity XFEL pulses, was particularly concerning. We therefore used very thin windows made from Kapton tape and minimized the scattering further by cutting with the FEL 100 × 100 μm^2 holes into the windows at the observation point (see Figure S1 in the SI). As detailed in the SI, these holes did not significantly affect nanodroplet freezing.

On the basis of the focused beam diameter, nozzle width, and particle number density, we estimate that each XFEL pulse interacted with ~25 particles. Although we worked with short, high-intensity X-ray pulses, it was not possible to observe diffraction using only single pulses. We only observed scattering from the ice crystals when we first averaged the "sample" data from ~36 000 X-ray pulses and then divided this by the average background from the same number of pulses. The background was determined by recording the scattering when the nozzle was fed with N_2 gas only. Further details of the averaging procedure are available in the SI. We note that even when using averaging, the diffuse scattering pattern expected from liquid drops could not be distinguished from the high scattering background.

Figure 2a shows the processed scattering signal as an average "image" of the CSPAD camera. The image shows three diffraction rings that we attribute to crystalline ice particles and additional spurious features whose origin is explained schematically in Figure 2b. The diffraction rings appeared only when water vapor flowed through the nozzle and only if the aerosol was probed at positions where our independent FTIR measurements showed that at least ~50% of the particles were frozen.

To identify the crystalline structure of the ice, we calculated the X-ray scattering spectrum by angularly averaging the 2D images over the regions of the detector not affected by the spurious effects indicated in Figure 2b. Figure 3 shows three spectra collected at different positions along the nozzle, corresponding to different temperatures. Each spectrum has distinct peaks, at q = 1.72, 2.79, and 3.27 $Å^{-1}$, values that are very close to those calculated for the (111), (220), and (311) peaks of cubic ice. A small peak near q = 2.3 $Å^{-1}$ in Figure 3a,c is entirely absent in Figure 3b; due to the weak and nonreproducible nature of the features near q = 2.3 $Å^{-1}$, we cannot identify them with the (102) peak of hexagonal ice at q = 2.35 $Å^{-1}$.

Given the lack of scattering peaks characteristic of hexagonal ice in our data, it is highly unlikely that the nanoparticles are comprised of this polymorph. We note that our spectra do not resolve the peak near q = 1.65 $Å^{-1}$ typically found in stacking-disordered ice.[15] This may be a consequence of diffraction peak broadening due to the small particle size, but it may also indicate that the structure of ice formed here is closer to that of pure cubic ice than the stacking-disordered ice produced in other experiments.

DOI: 10.1021/acs.jpclett.7b01142
J. Phys. Chem. Lett. 2017, 8, 3216–3222

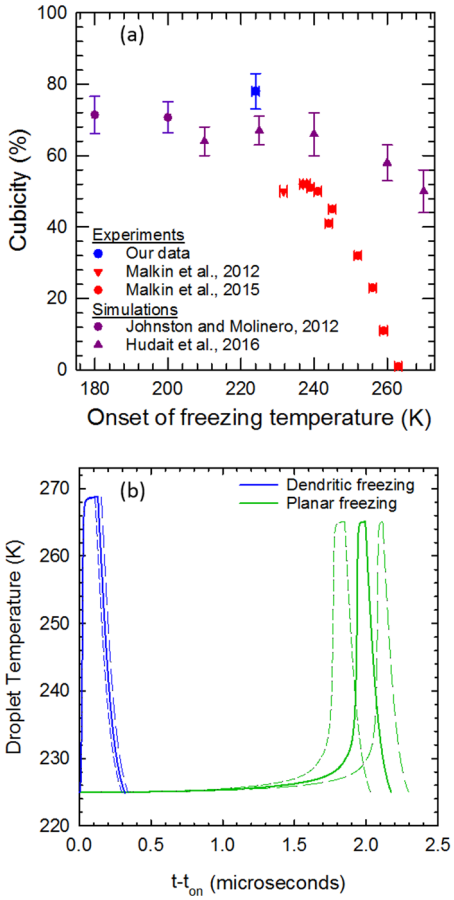

Figure 5. (a) The cubicity of ice I formed by freezing from supercooled water increases rapidly as the temperature at which the droplets froze decreases. Our result aligns well both with previous experimental data at higher temperatures and with the results of mW simulations. (b) The estimated temperature history of a freezing droplet is modeled by balancing the heat released by the phase transition against the heat removed by collisions with the carrier gas and the evaporation of water molecules. Calculations were made assuming a staged freezing mechanism that assumes either (i) dendritic ice growth at a velocity determined from a linear extrapolation of Pruppacher's[35] and Stan et al.'s[36] values or (ii) planar nanoscale ice growth at the velocity measured recently by Xu et al.[37] using a pulsed laser heating technique. Solid and dashed lines correspond, respectively, to the recommended and the limit values of the heat capacity of highly supercooled water from Murphy and Koop.[38]

To estimate the cubicity, χ, of the ice, we calculated the diffraction spectra expected in our experiments using the DIFFaX diffraction simulation,[15,33] accounting for peak broadening due to our small (r = 9.9 nm) average particle size[34] (see the SI for details). Figure 4a,b shows the expected scattering spectra for pure cubic and hexagonal ice nanoparticles, respectively. We then compared our experimental data to diffraction spectra calculated for different values of χ. We focused on the peak near q = 1.72 Å^{-1} because the peaks at higher q are weaker and their line shape is disorted more by shadowing effects. As illustrated in Figure 4c, values of χ up to 0.66 cannot match the shape of the first peak. Rather, as shown in Figure 4d–f, in all cases, χ for this ice is close to 0.8.

By fitting the experimental data with the predictions of the DIFFaX model and after taking into consideration the diffraction line broadening due to the particle size, we estimated a cubicity χ = 0.78 ± 0.05 (see the discussion and Figures S4 and S5 in the SI). Our cubicity estimate is significantly higher than the upper limit, typically $\chi \approx 0.5$, reported in previous experiments for freezing from liquid water.[15,18] Nevertheless, as illustrated in Figure 5a, our values are consistent both with the strong temperature dependence reported for χ in ice formed from supercooled water and with comparable mW simulations of Molinero and co-workers.[5,21,22] Our low freezing temperatures are the simplest explanation for the high cubicity but not the only possible one.

The small size of our drops may also play a role in increasing cubicity. Recent simulations suggest that the nanosized ice particles comparable in size to ours (15 nm) might have an *equilibrium* stacking disorder due to the entropic advantage of a more disordered structure.[39] Experiments on water frozen in nanopores showed that the ice becomes more cubic as the pore size decreases and does not seem to anneal to ice Ih.[40,41] The nanopore freezing experiments did not report cubicity values, but a comparison of the X-ray peak shapes indicates that water frozen in nanopores is less cubic than ours. The major differences between the nanopore experiments and ours are that (i) water in nanopores is in contact with a hydrophilic surface rather than with a gas, and thus the possible influence of the water's interface on nucleation and growth may be different, and (ii) the water in our droplets experiences a high Laplace pressure, on the order of 100 atm. The high pressure, according to Le Chatelier's principle, could favor the formation of highly cubic ice, which has higher density; experimentally, it was found that stacking-disordered ice with a high cubicity is ∼1% denser than the hexagonal ice.[42] We also note that simulations using multisite water potentials observed high rates of nucleation to cubic ice in the nanometer-sized subsurface region;[43,44] such a process, if still active at high Laplace pressures, may contribute to the high cubicity that we observed.

Another distinguishing feature of our experiment is the very short freezing time. Although the whole population of drops freezes in ∼45 μs, single drops freeze much more rapidly. To estimate this important time scale, we modeled the droplet's temperature during freezing assuming two limiting cases: (i) a rapid dendritic freezing mechanism as observed in micron-scale drops[45,46] and (ii) a slower planar ice growth as observed in a nanoscale experiment designed to rapidly dissipate the latent heat.[37] This model, described in the SI, predicts that the nanodrops will spend on the order of 100 ns at temperatures near the melting temperature and that freezing will take between ∼200 ns (dendritic freezing) and ∼2 μs (planar freezing). Because the duration of freezing and the time elapsed at temperatures near the melting point are orders of magnitude faster than the annealing times to hexagonal ice observed experimentally (minutes to hours), it is unlikely that significant annealing occurs during freezing, or up to the largest post-freezing delay that we investigated. Therefore, in our experiments, the cubicity should remain the same after freezing, and indeed, in Figure 4, the line shapes of the first diffraction peak are very similar.

The freezing of supercooled water is a complex process that illustrates the difficulty of characterizing and quantifying the formation of crystals under conditions that are far from equilibrium. Here, we showed that by combining a technique for producing deeply metastable samples with extremely rapid X-ray diffraction measurements one can study freezing under conditions approaching those used in simulations. We observed a feature that was predicted by simulations but was not

DOI: 10.1021/acs.jpclett.7b01142
J. Phys. Chem. Lett. 2017, 8, 3216–3222

previously observed in experiments: a high degree of cubicity. Perhaps more importantly, using an X-ray laser, we were able to probe the structure of ice less than 100 μs after its formation. In previous XFEL experiments that probed freezing after homogeneous ice nucleation in micron-sized droplets,[47,48] the shortest WAXS delays were approximately 1 ms; the ice structure was predominantly hexagonal (low cubicity), and shifts in the diffraction peaks indicated the heating of drops. In previous experimental studies using microemulsions,[15,16,49,50] the shortest WAXS delays were on the order of minutes, not sufficient to capture the short-term dynamics of solidification. Finally, in contrast to previous nanodroplet studies,[51] we have direct measurements of the droplet size, robust estimates of the droplet temperature, and a quantitative measure of the degree of cubicity of the ice produced. Our experimental approach offers a promising new avenue for understanding the initial stages of nonequilibrium freezing in supercooled water as well as other molecules.

■ ASSOCIATED CONTENT

Supporting Information

The Supporting Information is available free of charge on the ACS Publications website at DOI: 10.1021/acs.jpclett.7b01142.

Additional information about (i) XFEL cutting of beam apertures in the Kapton windows, (ii) processing of 2D scattering images, (iii) the comparison of data recorded from XFEL and synchrotron measurements, (iv) modeling of WAXS spectra and the determination of cubicity, and (v) evaluation of freezing duration in nanodrops (PDF)

■ AUTHOR INFORMATION

Corresponding Authors

*E-mail: wyslouzil.1@osu.edu (B.E.W.).
*E-mail: cstan@slac.stanford.edu (C.A.S.).

ORCID

Jonas A. Sellberg: 0000-0003-2793-5052
Claudiu A. Stan: 0000-0002-9809-4521
Barbara E. Wyslouzil: 0000-0001-9763-5990

Notes

The authors declare no competing financial interest.

■ ACKNOWLEDGMENTS

This work was supported by NSF Grants CHE-1213959 and CHE-1464924, by the U.S. Department of Energy, Office of Science, Chemical Sciences, Geosciences, and Biosciences Division, and by the SLAC Laboratory Directed Research and Development Program. Use of the Linac Coherent Light Source (LCLS), SLAC National Accelerator Laboratory, is supported by the U.S. Department of Energy, Office of Science, Office of Basic Energy Sciences under Contract No. DE-AC02-76SF00515. This research used resources of the Advanced Photon Source, a U.S. Department of Energy (DOE) Office of Science User Facility operated for the DOE Office of Science by Argonne National Laboratory under Contract No. DE-AC02-06CH11357. We thank S. Siefert, R. Winans, and J. Wölk for their help with the SAXS experiments. We thank Terry Anderson and Greg Stewart for assistance in preparation of the TOC figure and Figure 1b.

■ REFERENCES

(1) Ostwald, W. Studien Über Die Bildung und Umwandlung Fester Körper. 1. Abhandlung: Übersättigung und Überkaltung. *Z. Phys. Chem.* **1897**, *22U*, 289−330.
(2) Rein ten Wolde, P.; Frenkel, D. Homogeneous Nucleation and the Ostwald Step Rule. *Phys. Chem. Chem. Phys.* **1999**, *1*, 2191−2196.
(3) Herlach, D. M. Nonequilibrium Solidification of Undercooled Metallic Melts. *Mater. Sci. Eng., R* **1994**, *12*, 177−272.
(4) Rangno, A. L.; Hobbs, P. V. Ice Particle Concentrations and Precipitation Development in Small Polar Maritime Cumuliform Clouds. *Q. J. R. Meteorol. Soc.* **1991**, *117*, 207−241.
(5) Hudait, A.; Qiu, S. W.; Lupi, L.; Molinero, V. Free Energy Contributions and Structural Characterization of Stacking Disordered Ices. *Phys. Chem. Chem. Phys.* **2016**, *18*, 9544−9553.
(6) Murray, B. J.; Malkin, T. L.; Salzmann, C. G. The Crystal Structure of Ice Under Mesospheric Conditions. *J. Atmos. Sol.-Terr. Phys.* **2015**, *127*, 78−82.
(7) Kuhs, W. F.; Sippel, C.; Falenty, A.; Hansen, T. C. Extent and Relevance of Stacking Disorder in "Ice I(c)". *Proc. Natl. Acad. Sci. U. S. A.* **2012**, *109*, 21259−21264.
(8) Hudait, A.; Molinero, V. What Determines the Ice Polymorph in Clouds? *J. Am. Chem. Soc.* **2016**, *138*, 8958−8967.
(9) Salzmann, C. G.; Radaelli, P. G.; Slater, B.; Finney, J. L. The Polymorphism of Ice: Five Unresolved Questions. *Phys. Chem. Chem. Phys.* **2011**, *13*, 18468−18480.
(10) Murray, B. J.; Salzmann, C. G.; Heymsfield, A. J.; Dobbie, S.; Neely, R. R.; Cox, C. J. Trigonal Ice Crystals in Earth's Atmosphere. *Bull. Am. Meteorol. Soc.* **2015**, *96*, 1519−1531.
(11) Riikonen, M.; Sillanpaa, M.; Virta, L.; Sullivan, D.; Moilanen, J.; Luukkonen, I. Halo Observations Provide Evidence of Airborne Cubic Ice in the Earth's Atmosphere. *Appl. Opt.* **2000**, *39*, 6080−6085.
(12) Murray, B. J.; Knopf, D. A.; Bertram, A. K. The Formation of Cubic Ice Under Conditions Relevant to Earth's Atmosphere. *Nature* **2005**, *434*, 202−205.
(13) Shilling, J. E.; Tolbert, M. A.; Toon, O. B.; Jensen, E. J.; Murray, B. J.; Bertram, A. K. Measurements of the Vapor Pressure of Cubic Ice and their Implications for Atmospheric Ice Clouds. *Geophys. Res. Lett.* **2006**, *33*, L17801.
(14) Murphy, D. M. Dehydration in Cold Clouds is Enhanced by a Transition from Cubic to Hexagonal Ice. *Geophys. Res. Lett.* **2003**, *30*, 2230.
(15) Malkin, T. L.; Murray, B. J.; Brukhno, A. V.; Anwar, J.; Salzmann, C. G. Structure of Ice Crystallized from Supercooled Water. *Proc. Natl. Acad. Sci. U. S. A.* **2012**, *109*, 1041−1045.
(16) Murray, B. J.; Bertram, A. K. Formation and Stability of Cubic Ice in Water Droplets. *Phys. Chem. Chem. Phys.* **2006**, *8*, 186−192.
(17) Kuhs, W. F.; Bliss, D. V.; Finney, J. L. High-Resolution Neutron Powder Diffraction Study of Ice-Ic. *J. Phys., Colloq* **1987**, *48*, 631−636.
(18) Malkin, T. L.; Murray, B. J.; Salzmann, C. G.; Molinero, V.; Pickering, S. J.; Whale, T. F. Stacking Disorder in Ice I. *Phys. Chem. Chem. Phys.* **2015**, *17*, 60−76.
(19) Hansen, T. C.; Koza, M. M.; Kuhs, W. F. Formation and Annealing of Cubic Ice: I. Modelling of Stacking Faults. *J. Phys.: Condens. Matter* **2008**, *20*, 285104.
(20) Hansen, T. C.; Koza, M. M.; Lindner, P.; Kuhs, W. F. Formation and Annealing of Cubic Ice: II. Kinetic Study. *J. Phys.: Condens. Matter* **2008**, *20*, 285105.
(21) Moore, E. B.; Molinero, V. Is It Cubic? Ice Crystallization from Deeply Supercooled Water. *Phys. Chem. Chem. Phys.* **2011**, *13*, 20008−20016.
(22) Johnston, J. C.; Molinero, V. Crystallization, Melting, and Structure of Water Nanoparticles at Atmospherically Relevant Temperatures. *J. Am. Chem. Soc.* **2012**, *134*, 6650−6659.
(23) Li, T. S.; Donadio, D.; Russo, G.; Galli, G. Homogeneous Ice Nucleation from Supercooled Water. *Phys. Chem. Chem. Phys.* **2011**, *13*, 19807−19813.
(24) Haji-Akbari, A.; Debenedetti, P. G. Direct Calculation of Ice Homogeneous Nucleation Rate for a Molecular Model of Water. *Proc. Natl. Acad. Sci. U. S. A.* **2015**, *112*, 10582−10588.

DOI: 10.1021/acs.jpclett.7b01142
J. Phys. Chem. Lett. 2017, 8, 3216−3222

(25) Manka, A.; Pathak, H.; Tanimura, S.; Woelk, J.; Strey, R.; Wyslouzil, B. E. Freezing Water in No-Man's Land. *Phys. Chem. Chem. Phys.* **2012**, *14*, 4505−4516.
(26) Pathak, H.; Mullick, K.; Tanimura, S.; Wyslouzil, B. E. Nonisothermal Droplet Growth in the Free Molecular Regime. *Aerosol Sci. Technol.* **2013**, *47*, 1310−1324.
(27) Modak, V. P.; Pathak, H.; Thayer, M.; Singer, S. J.; Wyslouzil, B. E. Experimental Evidence for Surface Freezing in Supercooled n-Alkane Nanodroplets. *Phys. Chem. Chem. Phys.* **2013**, *15*, 6783−6795.
(28) Li, T. S.; Donadio, D.; Galli, G. Ice Nucleation at the Nanoscale Probes No Man's Land of Water. *Nat. Commun.* **2013**, *4*, 1887.
(29) Altarelli, M.; Mancuso, A. P. Structural Biology at the European X-ray Free-Electron Laser Facility. *Philos. Trans. R. Soc., B* **2014**, *369*, 20130311.
(30) Abbamonte, P.; Abild-Pedersen, F.; Adams, P.; Ahmed, M.; Albert, F.; Alonso Mori, R.; Anfinrud, P.; Aquila, A.; Armstrong, M.; Arthur, J.; et al. *New Science Opportunities Enabled by LCLS-II X-ray Lasers*; SLAC National Accelerator Laboratory: Menlo Park, CA, 2015; *SLAC-R-1053*, pp 3−189.
(31) Emma, P.; Akre, R.; Arthur, J.; Bionta, R.; Bostedt, C.; Bozek, J.; Brachmann, A.; Bucksbaum, P.; Coffee, R.; Decker, F. J.; et al. First Lasing and Operation of an Angstrom-Wavelength Free-Electron Laser. *Nat. Photonics* **2010**, *4*, 641−647.
(32) Liang, M. N.; Williams, G. J.; Messerschmidt, M.; Seibert, M. M.; Montanez, P. A.; Hayes, M.; Milathianaki, D.; Aquila, A.; Hunter, M. S.; Koglin, J. E.; et al. The Coherent X-ray Imaging instrument at the Linac Coherent Light Source. *J. Synchrotron Radiat.* **2015**, *22*, 514−519.
(33) Treacy, M. M. J.; Newsam, J. M.; Deem, M. W. A General Recursion Method for Calculating Diffracted Intensities from Crystals Containing Planar Faults. *Proc. R. Soc. London, Ser. A* **1991**, *433*, 499−520.
(34) Scherrer, P. Bestimmung der Größe und der Inneren Struktur von Kolloidteilchen Mittels Röntgenstrahlen. *Nachrichten Math. Phys.* **1918**, *2*, 98−100.
(35) Pruppacher, H. R. Interpretation of Experimentally Determined Growth Rates of Ice Crystals in Supercooled Water. *J. Chem. Phys.* **1967**, *47*, 1807−1813.
(36) Stan, C. A.; Schneider, G. F.; Shevkoplyas, S. S.; Hashimoto, M.; Ibanescu, M.; Wiley, B. J.; Whitesides, G. M. A Microfluidic Apparatus for the Study of Ice Nucleation in Supercooled Water Drops. *Lab Chip* **2009**, *9*, 2293−2305.
(37) Xu, Y. T.; Petrik, N. G.; Smith, S.; Kay, B. D.; Kimmel, G. A. Growth Rate of Crystalline Ice and the Diffusivity of Supercooled Water from 126 to 262 K. *Proc. Natl. Acad. Sci. U. S. A.* **2016**, *113*, 14921−14925.
(38) Murphy, D. M.; Koop, T. Review of the Vapour Pressures of Ice and Supercooled Water for Atmospheric Applications. *Q. J. R. Meteorol. Soc.* **2005**, *131*, 1539−1565.
(39) Lupi, L.; Hudait, A.; Peters, B.; Grunwald, M.; Mullen, R.; Nguyen, A.; Molinero, V. Role of Stacking Disorder in Ice Nucleation. Under review.
(40) Morishige, K.; Uematsu, H. The proper structure of cubic ice confined in mesopores. *J. Chem. Phys.* **2005**, *122*, 044711.
(41) Morishige, K.; Yasunaga, H.; Uematsu, H. Stability of Cubic Ice in Meospores. *J. Phys. Chem. C* **2009**, *113*, 3056−3061.
(42) Loerting, T.; Bauer, M.; Kohl, I.; Watschinger, K.; Winkel, K.; Mayer, E. Cryoflotation: Densities of Amorphous and Crystalline Ices. *J. Phys. Chem. B* **2011**, *115*, 14167−14175.
(43) Vrbka, L.; Jungwirth, P. Homogeneous Freezing of Water Starts in the Subsurface. *J. Phys. Chem. B* **2006**, *110*, 18126−18129.
(44) Haji-Akbari, A.; Debenedetti, P. G. Computational Investigation of Surface Freezing in a Molecular Model of Water. *Proc. Natl. Acad. Sci. U. S. A.* **2017**, *114*, 3316−3321.
(45) Hindmarsh, J. P.; Russell, A. B.; Chen, X. D. Experimental and Numerical Analysis of the Temperature Transition of a Suspended Freezing Water Droplet. *Int. J. Heat Mass Transfer* **2003**, *46*, 1199−1213.
(46) Buttersack, T.; Bauerecker, S. Critical Radius of Supercooled Water Droplets: On the Transition Toward Dendritic Freezing. *J. Phys. Chem. B* **2016**, *120*, 504−512.
(47) Laksmono, H.; McQueen, T. A.; Sellberg, J. A.; Loh, N. D.; Huang, C.; Schlesinger, D.; Sierra, R. G.; Hampton, C. Y.; Nordlund, D.; Beye, M.; et al. Anomalous Behavior of the Homogeneous Ice Nucleation Rate in "No-Man's Land". *J. Phys. Chem. Lett.* **2015**, *6*, 2826−2832.
(48) Sellberg, J. A.; Huang, C.; McQueen, T. A.; Loh, N. D.; Laksmono, H.; Schlesinger, D.; Sierra, R. G.; Nordlund, D.; Hampton, C. Y.; Starodub, D.; et al. Ultrafast X-ray Probing of Water Structure Below the Homogeneous Ice Nucleation Temperature. *Nature* **2014**, *510*, 381−384.
(49) Murray, B. J.; Bertram, A. K. Strong Dependence of Cubic Ice Formation on Droplet Ammonium to Sulfate Ratio. *Geophys. Res. Lett.* **2007**, *34*, L16810.
(50) Murray, B. J. Enhanced Formation of Cubic Ice in Aqueous Organic Acid Droplets. *Environ. Res. Lett.* **2008**, *3*, 025008.
(51) Huang, J.; Bartell, L. S. Kinetics of Homogeneous Nucleation in the Freezing of Large Water Clusters. *J. Phys. Chem.* **1995**, *99*, 3924−3931.

DOI: 10.1021/acs.jpclett.7b01142
J. Phys. Chem. Lett. 2017, 8, 3216−3222